Porous electrodes from self-assembled 3D jointed Pd polyhedra for direct formic acid fuel cells

Yang Li [a], Yichang Yan [a], Ming-Shui Yao [a], Feng Wang [b], Yanhong Li [a], Sean M. Collins [c], Yu-Lung Chiu [b], Shangfeng Du [a,*]

[a] School of Chemical Engineering, University of Birmingham, Birmingham B15 2TT, UK
[b] School of Metallurgy and Materials, University of Birmingham, Birmingham B15 2TT, UK
[c] School of Chemical and Process Engineering & School of Chemistry, University of Leeds, Leeds LS2 9JT, UK

ARTICLE INFO

ABSTRACT

The direct formic acid fuel cell (DFAFC) is recognized as a promising power source for its high electromotive force, easy fuel storage and transport. However, its power performance is low and the cost is high, which are known to originate from the sluggish formic acid oxidation (FAO) kinetics and poor mass transport within the DFAFC anode. Here, we present a new DFAFC anode design with a thin, porous, 3D-structured catalyst layer based on self-assembled jointed Pd polyhedra *in-situ* grown on the gas diffusion layer surface. The Pd polyhedra provide highly active jointed interfaces and high-index facets, boosting their catalytic activity towards FAO. The porous 3D catalyst layer facilitates the transport of reactants and products at the large current density region. Consequently, the present anode design exhibits a previously unachieved power density of 202 mW cm^{-2} at a Pd loading of 1.0 mg cm^{-2} in the HCOOH/air DFAFC test.

1. Introduction

The increasing global energy consumption and environmental pollution caused by fossil-fuel usage have prompted the accelerated development of clean energy technologies [1-4]. As an emerging sub-class of fuel cells (FCs), the direct formic acid fuel cell (DFAFC) has been acknowledged as one of the promising power sources for future portable electronic devices, benefiting from the high theoretical open circuit potential (OCP) (1.48 V, compared to 1.23 V of the hydrogen fuel cell and 1.21 V of the methanol fuel cell), and safe storage and easy transport of formic acid as a liquid fuel [5]. For a highpower performance DFAFC in practical applications, the key requirement is a catalytically active anode facilitating the sluggish formic acid reaction (FAO). Palladium (Pd) is by far regarded as the most active electrocatalyst for FAO and has received intensive attention. In particular, through several decades of development, the advance in nanostructured catalysts has brought about enormous progress in the DFAFC technology. Nevertheless, the state-of-the-art DFAFC still suffers from poor power performance and a high cost, which hinders its large-scale commercial implementation.

Current research activities in the DFAFC technology mainly revolve around the synthesis of highly active catalysts toward FAO by using nanostructured alloy (e.g., PtCu, PtPdAu, PdCu, PdSn, PtSnBi) together with controllable shapes (e.g., nanoplates, nanocubes, nanosheets, hemispheres, nanowires) [6-11]. Most of these studies are only limited to the half-cell electrochemical measurement employing the rotating disk electrode (RDE) technique in the liquid electrolyte [12,13]. Only a few have been applied to practical DFAFC electrodes, and the power performance reported is still unsatisfactory. For example, PdCu alloy nanosheet was reported with a high surface area (126.2 m^2/g$_{PdCu}$ compared to 16.5 m^2/g$_{Pd}$ of Pd black). Its intrinsic activity has also achieved greater than 10-fold improvement compared to commercial Pd catalysts (1493.5 mA mg$_{PdCu}^{-1}$ over 140.3 mA mg$_{Pd}^{-1}$) [9,14,15]. In contrast, the highest power density reported in the last decade is only 191 mW cm^{-2} for a DFAFC using a Bi-modified Pt catalyst in the formic acid/air single cell test, which is only 2.7 times higher than that of the commercial Pt/C catalyst [16-18]. With defect engineering, the intrinsic activity of Pd nanotube catalysts has been boosted to 3.65 A mg^{-1} toward FAO, but no electrode has been fabricated and evaluated with such a kind of catalyst in the single-cell test [8,19,20]. Therefore, the key challenge is how to bridge the gap by designing novel electrode structures constructed from defect-rich catalysts for DFAFCs with enhanced power performance [21-23].
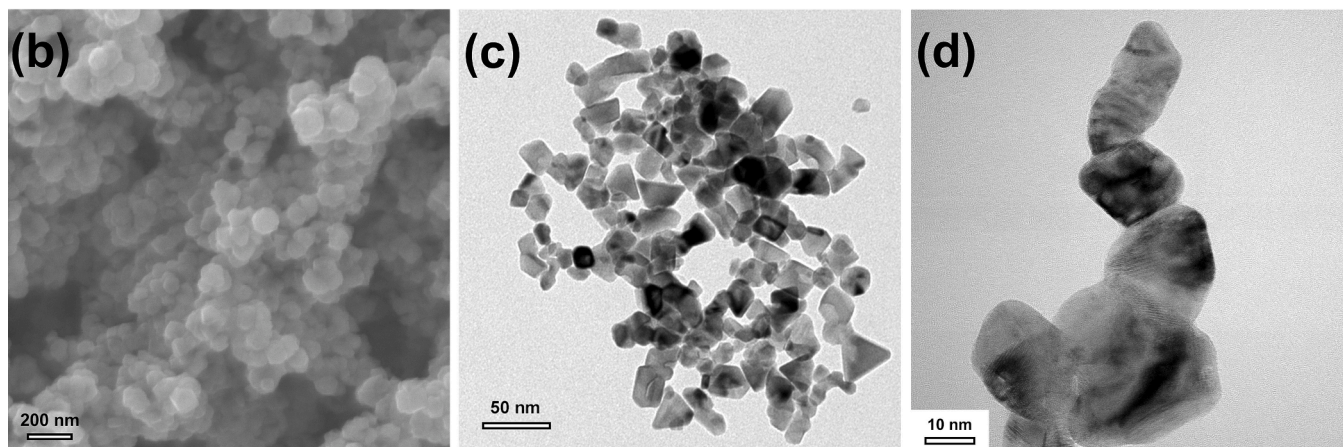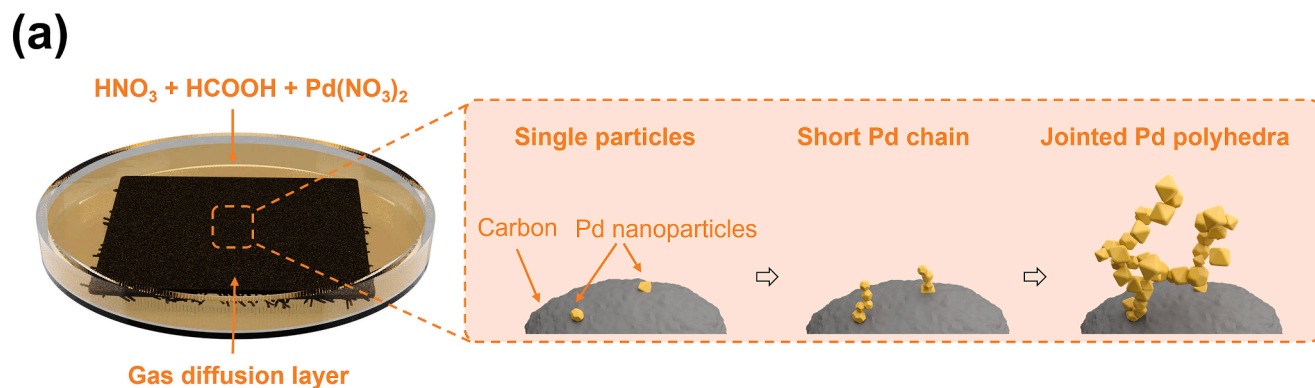
Fig. 1. Fabrication process and structural characterization of the jointed Pd polyhedron GDE. (a) Schematic illustration showing the preparation process. (b) A surface SEM image of the GDE. (c and d) TEM images of the scraped catalysts from the GDE.
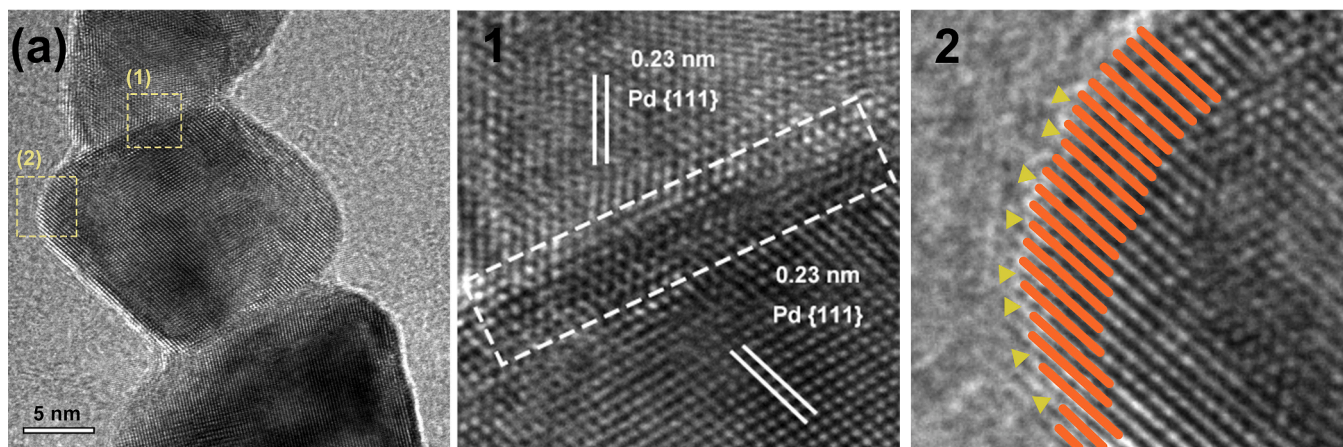
Fig. 2. (a) A HR-TEM image of jointed Pd polyhedra with two marked areas showing (1) the jointed interface and (2) edge of the lattice planes.

Herein, we demonstrate a new DFAFC anode design with a three-dimensional (3D) thin porous catalyst layer based on interconnected Pd polyhedra with defect-rich surfaces/interfaces. A facile one-pot approach is adopted for the *in-situ* growth of the Pd catalysts onto the gas diffusion layer (GDL) surface to fabricate the anode, using NO_3^- to control chemical reaction balance for modulating the crystal growth. The enhanced electrochemical surface area (ECSA) and superb stability of the electrode are verified in the gas diffusion electrode (GDE) test. A single cell is assembled at a catalyst loading of only 1.0 mg_{Pd} cm^{-2}, and a recorded power density of 202 mW cm^{-2} is achieved for the DFAFC in the formic acid/air test.

2. Material and methods

2.1. Materials

Sigracet 28 BC carbon paper gas diffusion layer (GDL) and Nafion® 212 membrane were purchased from Fuel Cell Store, USA. Palladium (II) nitrate hydrate solution ($Pd(NO_3)_2$, 10 wt% in 10 wt% HNO_3), and formic acid (HCOOH, $\geq$ 95%) were used as received from Sigma-Aldrich, UK. Nitric acid (HNO_3, 70%), ethanol and 2-propanol (IPA) were purchased from Fisher Scientific, UK. 10 wt% Nafion® dispersion (D1021) was supplied from Ion Power Inc., Germany. All H_2O was
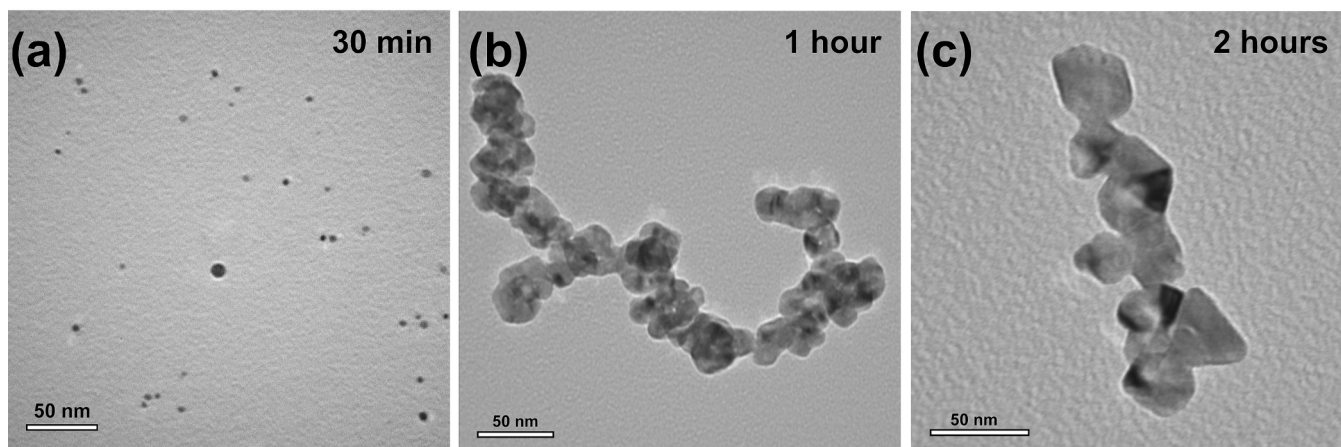
Fig. 3. Typical TEM images of the intermediate products collected at different intervals at 30 mins, 1 h and 2 h, revealing the formation of the jointed Pd polyhedron chain.

deionized using a Millipore water system (18 MΩ cm). The Pd/C catalyst (10 wt% on activated carbon support, Sigma-Aldrich, UK) was used as the benchmark catalyst. The Pt/C gas diffusion electrode (GDE) with a catalyst loading of 4.0 $mg_{Pt}\ cm^{-2}$ was purchased from Alfa Aesar, USA., and used as cathodes for fabricating all membrane electrode assemblies (MEAs).

2.2. Preparation of jointed Pd polyhedron gas diffusion electrodes

Pd polyhedron catalysts deposition on the carbon paper gas diffusion layer (GDL) surface was fabricated by an in-situ growth method: metal precursor, $Pd(NO_3)_2$, and reductant, HCOOH, were diluted by H_2O before being mixed in a petri dish, following by introducing concentrated HNO_3. A piece of GDL was then wetted with H_2O and IPA, and placed into the above solution. The petri dish was sealed and left to react in the fume cupboard for 48 h. The jointed Pd polyhedron GDE was obtained after being washed with H_2O and IPA, and dried under 40 °C for two hours. In order to study the influence of NO_3^- on the reaction rate and formed catalyst structure, reaction solution with six different HNO_3 concentrations was applied in this work, including Pd-1M, Pd-1.5M, Pd-2M, Pd-2.5M, Pd-3M and Pd-3.5M (the number after the hyphen indicates the molar concentration of HNO_3).

2.3. Physical characterization

The morphology of the GDE surface was observed using a Jeol 7000F scanning electron microscopy (SEM) with an accelerating voltage of 20 kV. To conduct transmission electron microscopy (TEM) analysis, catalysts were scraped from the GDE surface and then dispersed in ethanol by sonication before being loaded onto a 300 mesh Cu grid, and analyzed by using a Jeol 2100 TEM at 200 kV and a high-resolution TEM (HR-TEM) (FEI Talos F200 TEM, 200 kV). The crystal structure of the catalysts was determined by running X-ray diffraction (XRD) between 2θ values of 20-80° on a Bruker D8 Autosampler (Cu $K\alpha$ radiation, $\lambda = 0.15418$ nm). To analyze the chemical valences of the prepared catalysts, X-ray photoelectron spectroscopy (XPS) was run on a NEXSA spectrometer (Thermo Fisher Scientific) with a 72 W micro-focused monochromatic Al $K\alpha$ source, and results were corrected by using the C 1 s peak at 284.8 eV as a reference.

2.4. Ex-situ GDE half cell test

The ex-situ GDE half cell test is based on a three-electrode system that is assembled into a FlexCell polytetrafluoroethylene (PTFE, Gaskatel), as shown in Fig. S1. The working electrode was prepared by painting Nafion dispersion onto the GDE surface and dried under an infrared lamp. A commercial HydroFlex reference hydrogen electrode and a built-in platinum coil were used as the reference and counter electrode, respectively. Cyclic voltammetry (CV) scan was conducted in a 1.0 M $HClO_4$ aqueous electrolyte. N_2 gas was purged for at least 30 min to remove the O_2, followed by running 100 cycles of potential scan with a rate of 100 mV s^{-1} between 0.05 and 1.2 V vs RHE, and then three slow cycles (20 mV s^{-1}) were recorded for calculating electrochemical surface area (ECSA) of the electrode. To reveal the catalytic activity of the fabricated GDEs towards FAO, a similar scan was performed with 1.0 M $HClO_4$ containing 1.0 M HCOOH. Under the purge of N_2 gas, CV was recorded in the range of 0.2–1.2 V vs RHE with a scan rate of 20 mV s^{-1}. The durability of the GDE was monitored by the accelerated stress test (AST) with 1.0 M $HClO_4$. For this test, 1000 cycles of the potential scan between 0.05 and 1.2 V vs RHE (100 mV s^{-1}) were conducted to the GDE, and CV was recorded at the 1st, 500th and 1000th cycle with a scan rate of 20 mV s^{-1} for monitoring the degradation.

2.5. Membrane electrode assembly test

The as-prepared GDEs with an active area of 4 cm^2 and a catalyst loading of 1.0 $mg_{Pd}\ cm^{-2}$ were used as anodes for the DFAFC single cell test, on which diluted Nafion dispersion was painted at a loading of 1.8 mg cm^{-2}. A commercial Pt GDE with catalyst loading of 4.0 $mg_{Pt}\ cm^{-2}$ was used as the cathode. To fabricate MEA, anode, cathode and Nafion® 212 membrane were hot-pressed (135 °C, 4.9 MPa) for 2 min. The single cell test and electrochemical impedance spectroscopy (EIS) analyses were run with an 850e Multi-Range Fuel Cell Test System (Scribner Associates Inc., USA). 3 M HCOOH aqueous solution was fed into the anode at a flow rate of 1 mL min^{-1}, while dry air of 300 mL min^{-1} was supplied into the cathode without backpressure. Polarization curves were recorded between OCP and 0.1 V with a scan rate of 2 mV s^{-1} at 60 °C. The photos of the single cell test and a fabricated MEA are shown in Fig. S2.

3. Results and discussion

3.1. Electrode fabrication and structure

The GDE for the DFAFC anode was directly fabricated *via* an *in-situ* growth method (Fig. 1a). Generally, jointed Pd polyhedron catalysts were directly grown onto the GDL surface by reducing $Pd(NO_3)_2$ with HCOOH under the control of HNO_3 in aqueous solution. The reaction was left at room temperature for 48 h, followed by simple washing and drying process to obtain the Pd GDE (Fig. S3). An SEM image shows the catalyst layer structure in Fig. 1b, demonstrating a porous structure, built from compactly stacked Pd nanoparticles. In order to illustrate the
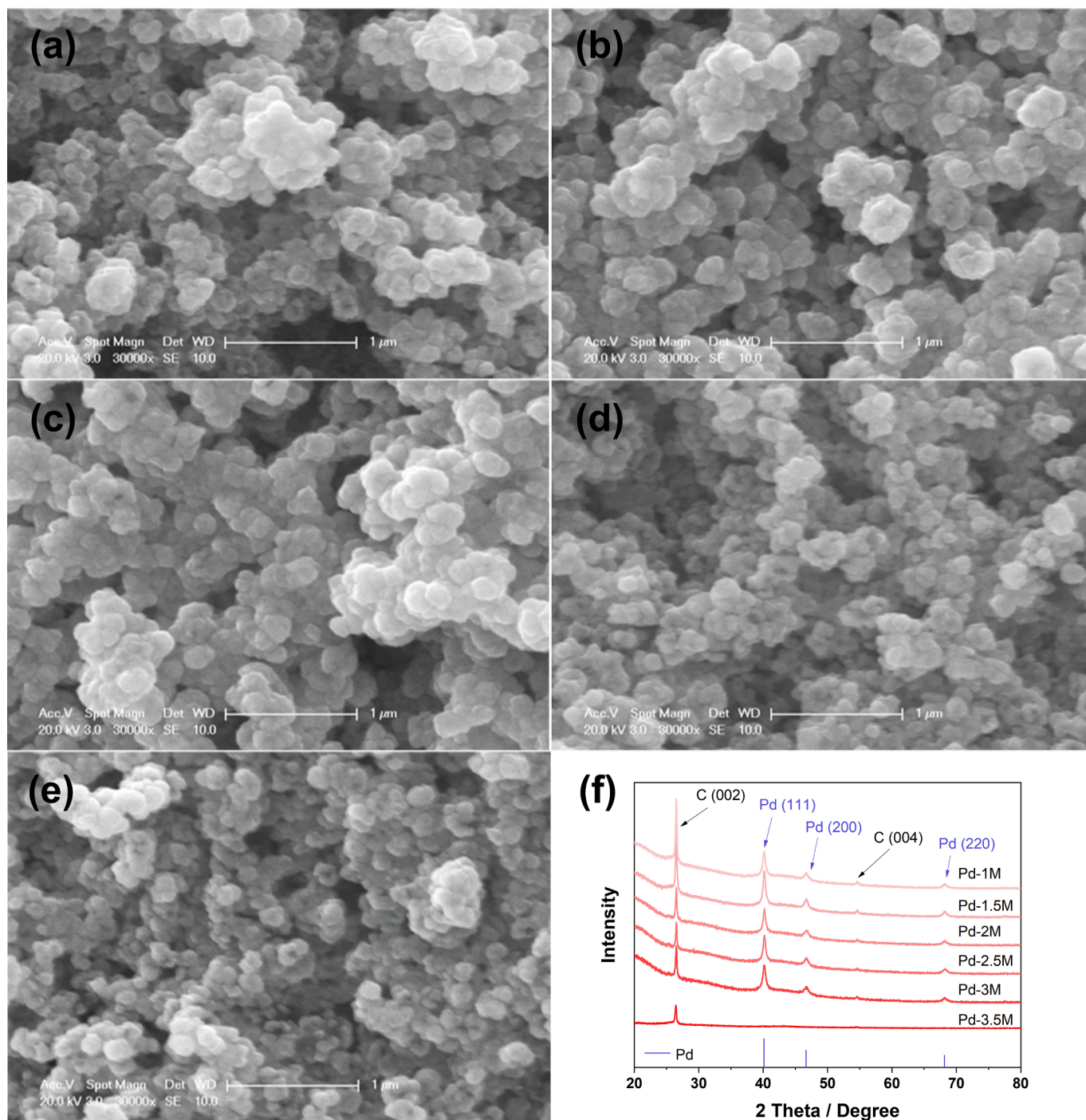
Fig. 4. (a to e) Surface SEM images and (f) XRD patterns of the as-fabricated Pd GDEs: (a) Pd-1M, (b) Pd-1.5M, (c) Pd-2M, (d) Pd-2.5M and (e) Pd-3M.

obtained Pd nanostructure, TEM analysis was performed on the catalysts scraped from the as-prepared GDE. Various polyhedra with an edge length of about 20–30 nm were observed (Fig. 1c and S4), including (i) tetrahedra, (ii) octahedra and (iii) decahedra, which are all covered by Pd{1 1 1} facets [19,24-26]. These nanostructures are linked up by co-planes and then assemble into short or long jointed Pd chains (Fig. 1d). Several chains/branches form a more extended network (Fig. 1c) and eventually lead to the formation of a porous catalyst layer with a 3D structure as observed in the SEM image (Fig. 1b). During the DFAFC operation, apart from the diffusion of formic acid to the catalytic sites on the catalyst surface, a large amount of CO_2 is also produced particularly at the large current density region [27]. This 3D porous

catalyst layer has a much smaller thickness of only about 1 μm as compared to 5–10 μm of the conventional one made from Pd nano-particles, as shown in Fig. S5, which can significantly facilitate the mass transport of both the reactant (formic acid) and also the product (CO_2), exhibiting a high potential to improve the fuel cell power performance.

To gain further insights into the jointed Pd chains, high-resolution TEM (HR-TEM) analysis was conducted. The obtained images (Fig. 2a) indicate the existence of jointed interfaces, and also steps on the edges of the polyhedra arising from the curved surface. As shown in Fig. 2a(1), rich lattice dislocations/defects are observed at the jointed interface of the adjacent two polyhedra. These are high surface energy domains and can serve as active sites to dramatically accelerate the adsorption and
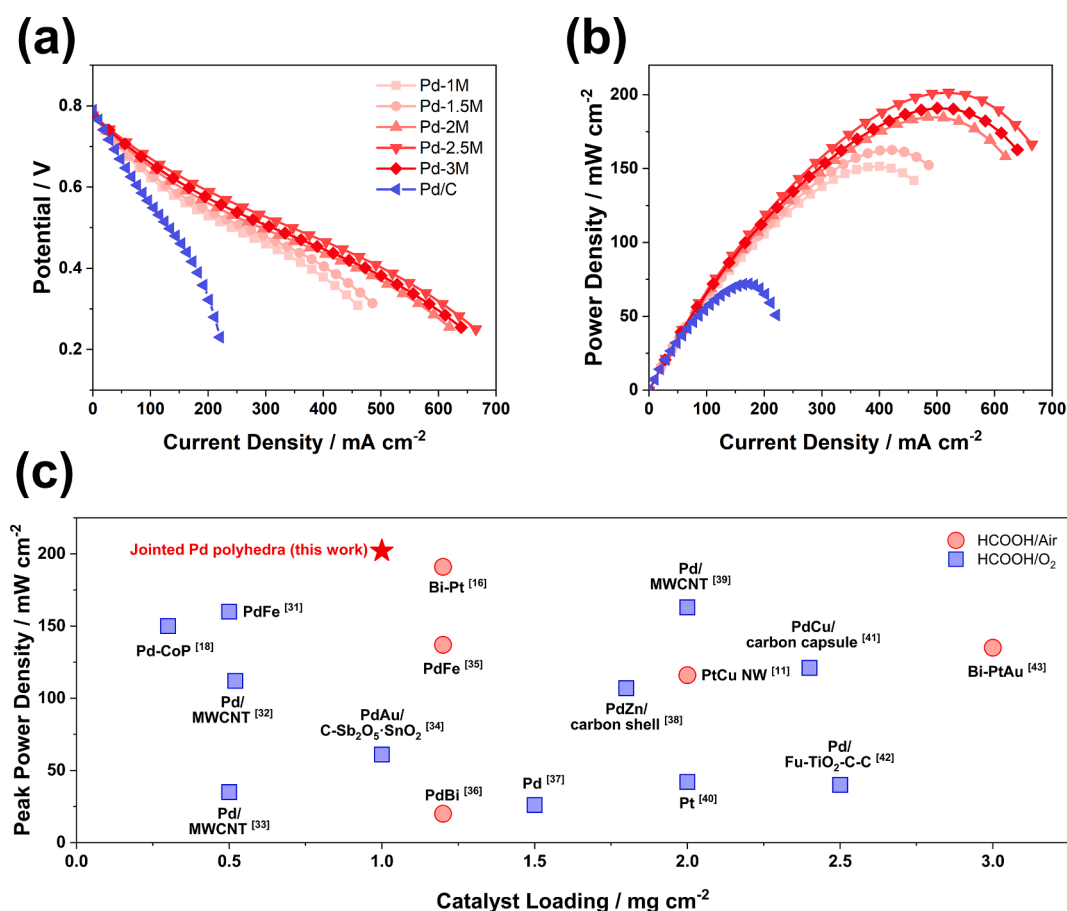
Fig. 5. DFAFC performance with various jointed Pd polyhedron GDEs and the Pd/C GDE as the anode. Test conditions: MEA active area: 4 cm^2, temperature: 60 °C, anode: 3 M formic acid at a flow rate of 1 mL min^{-1}, cathode: dry air with a flow rate of 300 mL min^{-1}. (a) polarization curves and (b) power density curves. (c) Comparison between the MEA with the jointed Pd polyhedron GDE (pentagram) and recently reported DFAFCs (solid circle representing the tests with air, and cube for the tests under oxygen) in terms of their peak power densities (Pd-CoP [18], PdFe [31], Pd/MWCNT [32], Pd/MWCNT [33], PdAu/C-Sb$_2$O$_5$·SnO$_2$ [34], Bi-Pt [16], PdFe [35], PdBi [36], Pd [37], PtZn/carbon shell [38], Pd/MWCNT [39], PtCu NW [11], Pt [40], PtCu/carbon capsule [41], Pd/Fu-TiO$_2$-C-C [42], Bi-PtAu [43]).

oxidation of formic acid [8,19,20]. Stepped high-index facets on the edge of a polyhedron (Fig. 2a(2)) also contribute to the catalytic activity improvement toward FAO as these facets can facilitate reaction through the direct oxidation pathway, and suppress the formation of poisoned intermediates [28-30]. The boosted mass transport characteristics of the 3D porous catalyst layer, and the promoted FAO catalytic activity resulting from the jointed interface and high-index facets, finally provide a chance to achieve a high power performance DFAFC anode for large current density operation.

To understand the formation and structural evolution of the Pd polyhedron chain, time-dependent experiments were conducted. The corresponding Pd nanostructures on the GDLs were collected at different intervals, and the obtained SEM and TEM images are shown in Fig. 3 and S6. After the reaction proceeds for 30 min, separately dispersed nanoparticles are observed with an average size of a few nanometres. A further reaction until 1 h leads to the formation of small particles with an average size of about 10 nm (Fig. 3b). It is worth noting that the Pd catalyst at this stage begins to self-assemble to form chain structures, and continuous lattice fringes are also shown between the adjacent particles due to the successively deposited Pd atoms at the interface between two contacted nanoparticles by further reducing Pd ions in the solution (Fig. S7). As the reaction goes on for 2 h, these nanoparticles within the chain grow larger with the continued reduction of Pd ions, finally resulting in the formation of the jointed polyhedron structure (Fig. 3c). The surface SEM analysis indicates the self-assembled polyhedron structures grown on the surface of the GDL, and partly covering the carbon nanosphere surface at this point (Fig. S6a). However, the

colour of the solution after two hours is still yellow, although it is much lighter than that at the beginning, indicating a continued growing process is still required to fully reduce the Pd precursor. As the reaction carries on to 4, 6 and 8 h, more precursor is consumed, and the solution colour becomes lighter until it becomes nearly colourless at 8 h. More polyhedra are formed and cover the majority of the GDL surface (Fig. S6, b to d).

The selection of the Pd precursor and the concentration of NO$_3^-$ are two key factors in subtly controlling the formation of the jointed Pd polyhedra. Due to the relatively low standard reduction potential ($E° = +0.59$ V vs SHE), it is difficult to reduce the most common precursor, $[PdCl_4]^{2-}$ (including H$_2$PdCl$_4$, Na$_2$PdCl$_4$, and K$_2$PdCl$_4$), by formic acid ($E° = +0.25$ V vs SHE), especially in high loading applications as required her for the DFAFC anode. Thus, Pd^{2+} (PdNO$_3$) with a higher $E°$ (+0.951 V vs SHE) was selected as the precursor. However, the large $\Delta E°$ between Pd^{2+} and formic acid results in an ultra-fast reduction rate that occurs in the solution through homogeneous nucleation and crystal growth. As a result, the Pd particles are formed in the solution and then settle down onto the GDL surface (Fig. S8a), finally developing into loosely stacked tree-like Pd crystals with features sizes on the micron scale (Fig. S9), which can easily be washed away from the GDL surface and cannot be used as a practical electrode. To slow down the reduction rate, NO$_3^-$ was introduced to modulate crystal growth by controlling the chemical reaction balance (Pd(NO$_3$)$_2$ + HCOOH → Pd + CO$_2$↑ + 2HNO$_3$). A mixed solution containing water, HCOOH, Pd(NO$_3$)$_2$ and HNO$_3$ (Pd-2.5M, 2.5 M represents the concentration of HNO$_3$ in the mixed solution) was left to react for 24 h, during which the color of the
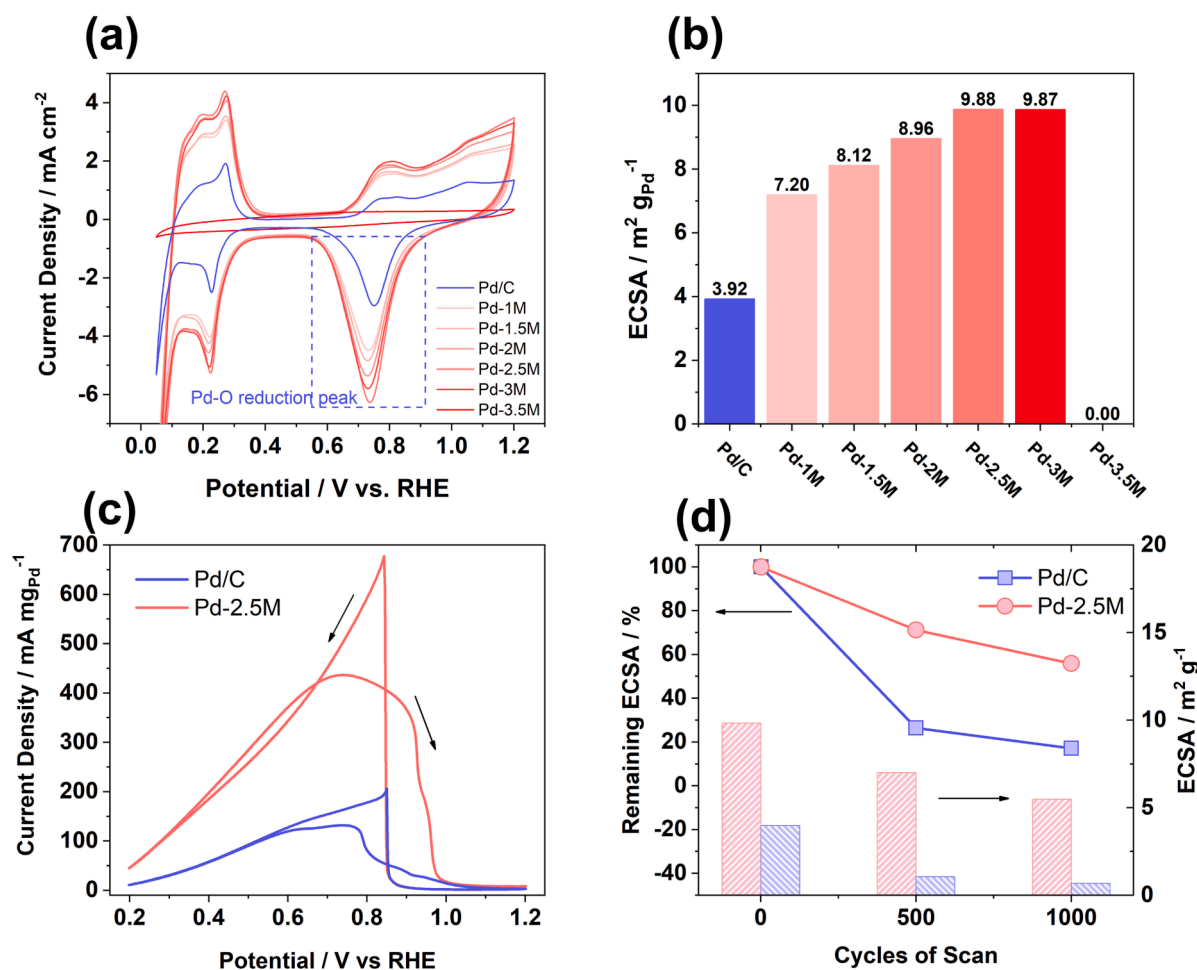
Fig. 6. Ex-situ GDE test of various jointed Pd polyhedron GDEs and the Pd/C GDE. (a) CV plots in 1.0 M $HClO_4$ with a scan rate of 20 mV s^{-1}. (b) Comparison of the ECSA for all GDEs calculated from the Pd-O reduction peaks in (a). (c) CV curves in $HClO_4$ (1.0 M aqueous solution) containing HCOOH (1.0 M) with a scan rate of 20 mV s^{-1}. (d) Change of the ECSA with the potential scan cycle.

solution changed from yellow to colorless, and no solid catalyst was observed in the solution or on the glassware (Fig. S8b). This result suggests most Pd precursor is reduced and grow onto the GDL surface. XPS analysis (Fig. S10) confirms that the formed Pd catalyst is effectively reduced to its metallic state Pd(0) greater than 99%. Pd GDEs fabricated with various HNO_3 concentrations from 1 to 3.5 M are compared in Fig. 4. The results show that the nanosized Pd particles tend to form agglomerates at a low HNO_3 concentration (1 M or 1.5 M). Whereas, there's no peak of Pd detected from the XRD pattern at a HNO_3 concentration of 3.5 M, demonstrating the reaction nearly stops at such a high concentration (Fig. S8c). Thus, the optimal concentration is determined 2.5 M, where fewer aggregates are formed on the GDL surface (Fig. 4d), and a desirable surface cover is also achieved.

3.2. Electrode performance

The single-cell test was conducted in HCOOH/air for the membrane electrode assemblies (MEAs) fabricated with the as-prepared jointed Pd polyhedron GDEs and Pd/C GDE with a catalyst loading of 1.0 mg$_{Pd}$ cm^{-2} as the anodes. The recorded polarization and power density curves are shown in Fig. 5a and 5b, respectively. Compared to the DFAFC with the Pd/C GDE, all the as-prepared jointed Pd polyhedron GDEs show a much higher power density across the whole current density range. At the large current density region close to 700 mA cm^{-2}, all MEAs with the Pd GDEs fabricated with HNO_3 above 2 M also display a very slow voltage drop, demonstrating excellent mass transfer characteristics with

little concentration loss. These improvements are further confirmed with the much smaller semicircle with the EIS pattern recorded at 0.5 V (Fig. S11), revealing the improved kinetic activities and significantly reduced mass transport resistance. This enables a good possibility for delivering a high power density electrode. The MEA with Pd-2.5 M GDE records a current density of 491.3 mA cm^{-2} at 0.4 V and achieves a peak power density of 202 mW cm^{-2}, outperforming other jointed Pd polyhedron GDEs, and it is 2.8 folds of the Pd/C GDE (71.9 mW cm^{-2}). Considering a comparable low catalyst loading of 1.0 mg$_{Pd}$ cm^{-2} and the HCOOH/air testing condition, the power density achieved here is the best among the recently reported DFAFCs (Fig. 5c), especially only mono-metal Pd is used without employing any support or alloying metal.

To explore the performance enhancement mechanisms of the jointed Pd polyhedron GDE, the ex-situ GDE half-cell test was also performed with the as-prepared and benchmark GDEs. Fig. 6a shows the cyclic voltammetry (CV) plots recorded in 1.0 M $HClO_4$ aqueous electrolyte. The electrochemical surface area (ECSA) values were determined from the Pd-O reduction peak and compared in Fig. 6b. The ECSA of Pd-2.5 M GDE reaches 9.88 m^2 g$_{Pd}^{-1}$, much higher than the Pd/C GDE (3.92 m^2 g$_{Pd}^{-1}$), confirming the advantage of the porous electrode formed by the jointed polyhedron nanostructures. The ECSA increases with the increasing HNO_3 concentration from 1.0 M to 2.5 M, and no significant change of ECSA is observed when the concentration is further increased to 3.0 M. Thus, based on the ECSA, the optimal HNO_3 concentration for Pd reduction is also determined at 2.5 M, which is consistent with the
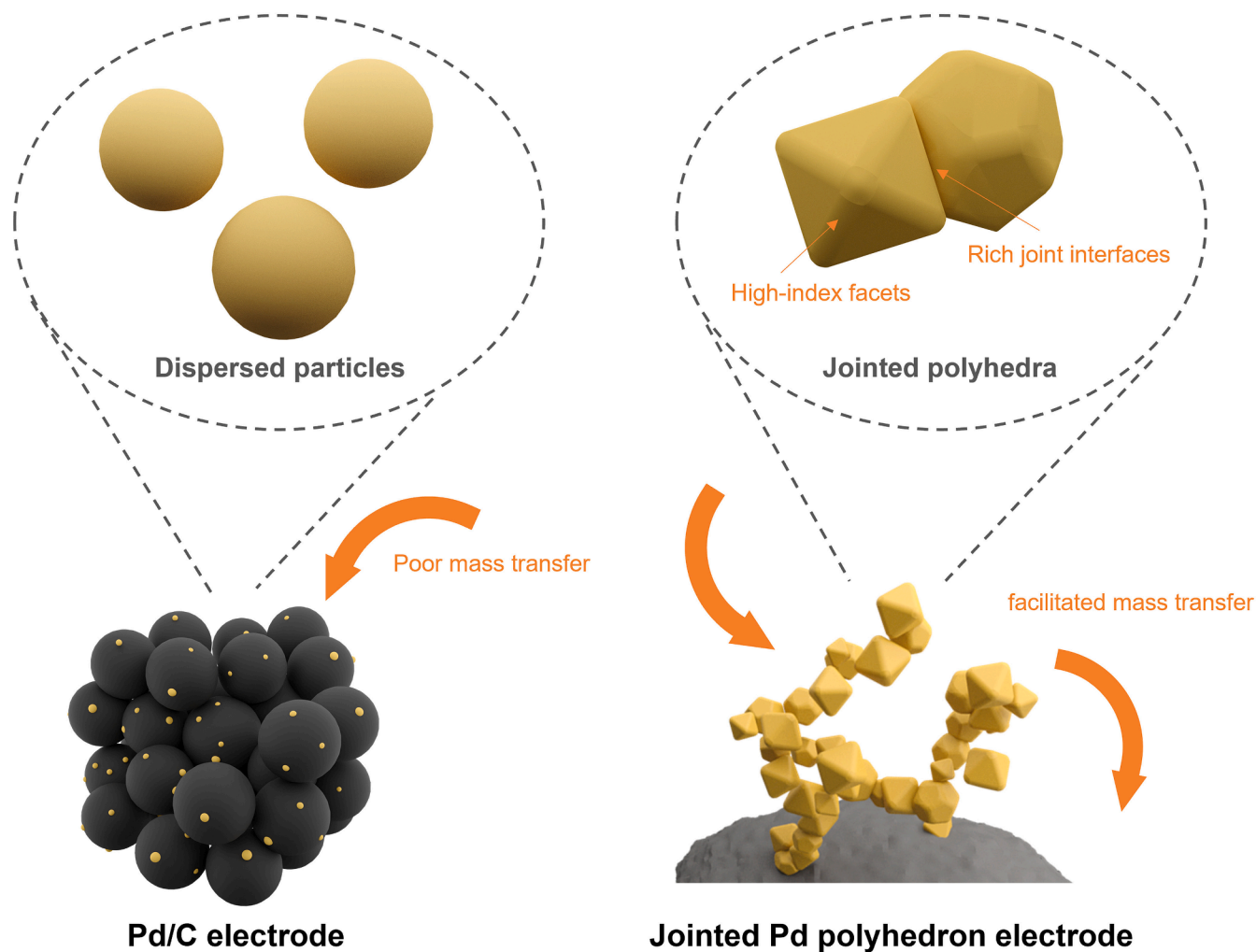
Fig. 7. Illustration of the Pd/C GDE and jointed Pd polyhedron GDE.

condition determined above based on the physical characterization results. Eventually, when the HNO_3 concentration arrives at 3.5 M (Pd-3.5 M), there is no Pd-related peak detected on the CV curve, indicating that there is no catalyst formed on the GDL surface. This is in line with the XRD analysis results (Fig. 4f). The large ECSA of the jointed Pd polyhedron GDE suggests rich active sites available for FAO within the electrode. To compare the mass activity towards FAO of Pd-2.5 M and the Pd/C GDEs, the CV measurement was also performed in $HClO_4$ + HCOOH electrolyte (Fig. 6c). Pd-2.5 M GDE shows a mass activity of 677.2 mA mg_{Pd}^{-1}, which is ~3.3 times higher than that of the Pd/C GDE.

The durability of Pd-2.5 M GDE was evaluated by accelerated stress testing (AST) via 1000 cycles of potential scan in the ex-situ GDE half cell test (Fig. S12). The ECSA changes are summarized and compared to the Pd/C GDE in Fig. 6d. A significant ECSA drop occurs to the Pd/C GDE within the first 500 cycles, and only about 25% of the initial ECSA is retained. This fast degradation can be ascribed to commonly agreed Pd dissolution in the acidic electrolyte [44,45], and is also affected by the catalyst aggregation and Ostwald ripening. On the other hand, Pd-2.5 M GDE shows a much lower decline rate, remaining about 75% of the initial ECSA after the first 500 cycles. This improved stability of the jointed Pd polyhedron GDE can be attributed to the GDE fabrication approach and the jointed polyhedron nanostructure. The GDE prepared by the *in-situ* growth method enables strong binding between the catalyst structures and substrate to form a durable electrode structure, which is also shown by the retained similar surface morphology after AST (Fig. S13). Furthermore, the Pd polyhedra are built by the most stable Pd

{1 1 1} facets and linked by the jointed interface, providing a stable nanostructure. With the GDE from the conventional Pd/C nanoparticles, the catalyst ink was sprayed onto the GDL surface. The weak catalyst/support and catalyst/catalyst contact can potentially cause severe catalyst loss during the cycling testing, especially for this practice with a thick catalyst layer because of the high catalyst loading. Accordingly, an ECSA loss of 82.8% is recorded for the Pd/C GDE compared to 44.1% of the Pd-2.5 M GDE after the AST.

The jointed Pd polyhedron GDE demonstrated excellent catalytic power performance and durability as the anode in the DFAFC test. Its advantage is contributed by the unique nano- and micro-structures of the fabricated electrode (Fig. 7). The jointed Pd polyhedra are enclosed by Pd{1 1 1} facets (Fig. 2a(1)). Their catalytic activity is boosted by the highly active jointed interfaces [21,46,47] and the high-index facets on the edge of the polyhedra, which include the high density of atomic steps, edges, kinks and dangling bonds [48-50]. The density functional theory (DFT) calculation reveals that the high index facets suppress the formation of poisoned intermediates during the fuel cell operation, thus facilitating the direct pathway of FAO for a high-performance DFAFC [28]. Notably, the high-index facets are also exposed at the twin boundaries of the decahedron and icosahedron. These shapes are deemed to form from several tetrahedral units, in which twin boundaries are necessary to bridge different units [19]. When the catalyst layer is constructed through the self-assembling of these nanostructures, a 3D interconnected porous structure is achieved at a much thinner layer that allows for more thorough exposure of the intrinsic active sites and the

rapid transport of the reactants (formic acid) and products (CO_2), thus maximizing the catalyst utilization for a large ECSA (Fig. 6b). In comparison, a conventional Pd/C GDE is usually prepared by directly spraying the catalyst ink onto a substrate (GDL or membrane). The formed catalyst layer is finished with randomly packed catalyst nanoparticles and a relatively dense structure (Fig. S14). As a result of which, a large mass transport resistance is usually observed with Pd/C GDEs, and it is further worsened by the very thick catalyst layer at a high catalyst loading and also multi-phase (liquid and gas) transfer, such as in the DFAFC [51,52]. Therefore, compared to the Pd/C electrode, the jointed Pd polyhedron electrode not only boosts the available amount of highly active catalytic sites, but also promotes the transport of both formic acid fuel and the produced CO_2 during the fuel cell operation, finally delivering high power performance.

4. Conclusion

A jointed Pd polyhedron GDE design is demonstrated with a facile one-step wet chemical fabrication process using the formic acid reduction method in aqueous solution at room temperature. In particular, NO_3^- was introduced to control the chemical balance of the reaction to provide a suitable reduction rate for crystal growth. The self-assembling of the jointed polyhedra formed a thin 3D porous catalyst layer structure. The highly active jointed interfaces and the high-index facets of the polyhedra led to a larger ECSA with better catalytic activity towards FAO compared to the Pd/C electrode in the GDE half-cell test, as well as better stability due to the polyhedron structure. Together with the promoted mass transport characteristics of the thin 3D porous catalyst layer, the MEA with the jointed Pd polyhedron GDE as the anode recorded a power density of up to 202 mW cm^{-2}, demonstrating the great potential for practical application. This concept for electrode design is not restricted to the DFAFC, and can be transferred to other kinds of liquid-involved electrochemical devices. The approach would also be applicable for Pd alloy polyhedra, which in turn would lead to even further enhanced performance due to increased activity of Pd alloys.

Declaration of Competing Interest

The authors declare that they have no known competing financial interests or personal relationships that could have appeared to influence the work reported in this paper.

Data availability

Data will be made available on request.

Acknowledgements

Appendix A. Supplementary data

Supplementary data to this article can be found online at https://doi.org/10.1016/j.cej.2023.142244.

References

[1] H. Tang, Y. Su, B. Chi, J. Zhao, D. Dang, X. Tian, S. Liao, G.-R. Li, Nodal PtNi nanowires with Pt skin and controllable Near-Surface composition for enhanced oxygen reduction electrocatalysis in fuel cells, Chem. Eng. J. 418 (2021), 129322, https://doi.org/10.1016/j.cej.2021.129322.

[2] Y. Liu, W. Xue, S. Seo, X. Tan, D. Mei, C. Liu, I.-S. Nam, S.B. Hong, Water: A promoter of ammonia selective catalytic reduction over copper-exchanged LTA zeolites, Appl. Catal. B Environ. 294 (2021), 120244, https://doi.org/10.1016/j.apcatb.2021.120244.

[3] I. Heo, S. Sung, M.B. Park, T.S. Chang, Y.J. Kim, B.K. Cho, S.B. Hong, J.W. Choung, I.-S. Nam, Effect of hydrocarbon on DeNOx Performance of selective catalytic reduction by a combined reductant over Cu-containing zeolite catalysts, ACS Catal. 9 (2019) 9800–9812, https://doi.org/10.1021/acscatal.9b02763.

[4] R. Tan, A. Wang, R. Malpass-Evans, R. Williams, E.W. Zhao, T. Liu, C. Ye, X. Zhou, B.P. Darwich, Z. Fan, L. Turcani, E. Jackson, L. Chen, S.Y. Chong, T. Li, K.E. Jelfs, A.I. Cooper, N.P. Brandon, C.P. Grey, N.B. McKeown, Q. Song, Hydrophilic microporous membranes for selective ion separation and flow-battery energy storage, Nat. Mater. 19 (2020) 195–202, https://doi.org/10.1038/s41563-019-0536-8.

[5] Y. Li, Y. Yan, S. Du, Liquid fueled fuel cells, in: Compr. Renew. Energy, Elsevier, 2022: pp. 399–419. 10.1016/B978-0-12-819727-1.00110-2.

[6] S. Luo, W. Chen, Y. Cheng, X. Song, Q. Wu, L. Li, X. Wu, T. Wu, M. Li, Q. Yang, K. Deng, Z. Quan, Trimetallic synergy in intermetallic PtSnBi nanoplates boosts formic acid oxidation, Adv. Mater. 31 (2019) 1903683, https://doi.org/10.1002/adma.201903683.

[7] C. Rettenmaier, R.M. Arán-Ais, J. Timoshenko, R. Rizo, H.S. Jeon, S. Kühl, S. W. Chee, A. Bergmann, B. Roldan Cuenya, Enhanced formic acid oxidation over SnO 2 -decorated Pd nanocubes, ACS Catal. 10 (2020) 14540–14551, https://doi.org/10.1021/acscatal.0c03212.

[8] J. Ding, Z. Liu, X. Liu, J. Liu, Y. Deng, X. Han, C. Zhong, W. Hu, Mesoporous decoration of freestanding palladium nanotube arrays boosts the electrocatalysis capabilities toward formic acid and formate oxidation, Adv. Energy Mater. 9 (2019) 1900955, https://doi.org/10.1002/aenm.201900955.

[9] N. Yang, Z. Zhang, B. Chen, Y. Huang, J. Chen, Z. Lai, Y. Chen, M. Sindoro, A.-L. Wang, H. Cheng, Z. Fan, X. Liu, B. Li, Y. Zong, L. Gu, H. Zhang, Synthesis of ultrathin PdCu alloy nanosheets used as a highly efficient electrocatalyst for formic acid oxidation, Adv. Mater. 29 (2017) 1700769, https://doi.org/10.1002/adma.201700769.

[10] W. Liang, Y. Wang, L. Zhao, W. Guo, D. Li, W. Qin, H. Wu, Y. Sun, L. Jiang, 3D anisotropic Au@Pt–Pd hemispherical nanostructures as efficient electrocatalysts for methanol, ethanol, and formic acid oxidation reaction, Adv. Mater. 33 (2021) 2100713, https://doi.org/10.1002/adma.202100713.

[11] Y. Li, Y. Yan, Y. He, S. Du, Catalyst electrodes with PtCu nanowire arrays in situ grown on gas diffusion layers for direct formic acid fuel cells, ACS Appl. Mater. Interfaces. 14 (2022) 11457–11464, https://doi.org/10.1021/acsami.1c24010.

[12] D. Banham, S. Ye, Current status and future development of catalyst materials and catalyst layers for proton exchange membrane fuel cells: an industrial perspective, ACS Energy Lett. 2 (2017) 629–638, https://doi.org/10.1021/acsenergylett.6b00644.

[13] C.-Y. Ahn, J.E. Park, S. Kim, O.-H. Kim, W. Hwang, M. Her, S.Y. Kang, S. Park, O. J. Kwon, H.S. Park, Y.-H. Cho, Y.-E. Sung, Differences in the electrochemical performance of Pt-based catalysts used for polymer electrolyte membrane fuel cells in liquid half- and full-cells, Chem. Rev. 121 (2021) 15075–15140, https://doi.org/10.1021/acs.chemrev.0c01337.

[14] Y. Xie, N. Dimitrov, Ultralow Pt loading nanoporous Au-Cu-Pt thin film as highly active and durable catalyst for formic acid oxidation, Appl. Catal. B Environ. 263 (2020), 118366, https://doi.org/10.1016/j.apcatb.2019.118366.

[15] H. Fan, M. Cheng, L. Wang, Y. Song, Y. Cui, R. Wang, Extraordinary electrocatalytic performance for formic acid oxidation by the synergistic effect of Pt and Au on carbon black, Nano Energy 48 (2018) 1–9, https://doi.org/10.1016/j.nanoen.2018.03.018.

[16] M. Choi, C.-Y. Ahn, H. Lee, J.K. Kim, S.-H. Oh, W. Hwang, S. Yang, J. Kim, O.-H. Kim, I. Choi, Y.-E. Sung, Y.-H. Cho, C.K. Rhee, W. Shin, Bi-modified Pt supported on carbon black as electro-oxidation catalyst for 300 W formic acid fuel cell stack, Appl. Catal. B Environ. 253 (2019) 187–195, https://doi.org/10.1016/j.apcatb.2019.04.059.

[17] J. Lai, W. Niu, S. Li, F. Wu, R. Luque, G. Xu, Concave and duck web-like platinum nanopentagons with enhanced electrocatalytic properties for formic acid oxidation, J. Mater. Chem. A. 4 (2016) 807–812, https://doi.org/10.1039/C5TA08882H.

[18] L. Feng, J. Chang, K. Jiang, H. Xue, C. Liu, W.-B. Cai, W. Xing, J. Zhang, Nanostructured palladium catalyst poisoning depressed by cobalt phosphide in the electro-oxidation of formic acid for fuel cells, Nano Energy. 30 (2016) 355–361, https://doi.org/10.1016/j.nanoen.2016.10.023.

[19] S.-I. Choi, J.A. Herron, J. Scaranto, H. Huang, Y. Wang, X. Xia, T. Lv, J. Park, H.-C. Peng, M. Mavrikakis, Y. Xia, A comprehensive study of formic acid oxidation on palladium nanocrystals with different types of facets and twin defects, ChemCatChem. 7 (2015) 2077–2084, https://doi.org/10.1002/cctc.201500094.

[20] W. Li, D. Wang, Y. Zhang, L. Tao, T. Wang, Y. Zou, Y. Wang, R. Chen, S. Wang, Defect engineering for fuel-cell electrocatalysts, Adv. Mater. 32 (2020) 1907879, https://doi.org/10.1002/adma.201907879.

[21] X. Tian, X. Zhao, Y.-Q. Su, L. Wang, H. Wang, D. Dang, B. Chi, H. Liu, E.J. M. Hensen, X.W.(. Lou, B.Y. Xia, Engineering bunched Pt-Ni alloy nanocages for efficient oxygen reduction in practical fuel cells, Science 366 (6467) (2019) 850–856.

[22] M. Li, Z. Zhao, T. Cheng, A. Fortunelli, C.-Y. Chen, R. Yu, Q. Zhang, L. Gu, B. V. Merinov, Z. Lin, E. Zhu, T. Yu, Q. Jia, J. Guo, L. Zhang, W.A. Goddard, Y. u. Huang, X. Duan, Ultrafine jagged platinum nanowires enable ultrahigh mass activity for the oxygen reduction reaction, Science 354 (6318) (2016) 1414–1419.

[23] T. Lazaridis, B.M. Stühmeier, H.A. Gasteiger, H.A. El-Sayed, Capabilities and limitations of rotating disk electrodes versus membrane electrode assemblies in the investigation of electrocatalysts, Nat. Catal. 5 (2022) 363–373, https://doi.org/ 10.1038/s41929-022-00776-5.

[24] B. Lim, Y. Xiong, Y. Xia, A water-based synthesis of octahedral, decahedral, and icosahedral Pd nanocrystals, Angew. Chem., Int. Ed. 46 (2007) 9279–9282, https://doi.org/10.1002/anie.200703755.

[25] G. Fu, X. Jiang, L. Ding, L. Tao, Y. Chen, Y. Tang, Y. Zhou, S. Wei, J. Lin, T. Lu, Green synthesis and catalytic properties of polyallylamine functionalized tetrahedral palladium nanocrystals, Appl. Catal. B Environ. 138–139 (2013) 167–174, https://doi.org/10.1016/j.apcatb.2013.02.052.

[26] M. Chen, B. Wu, J. Yang, N. Zheng, Small adsorbate-assisted shape control of Pd and Pt nanocrystals, Adv. Mater. 24 (2012) 862–879, https://doi.org/10.1002/ adma.201104145.

[27] S. Osman, M. Ahmed, Enhancing the performance of direct methanol fuel cells via a new anode design for carbon dioxide bubbles removal, Energy Convers. Manag. 251 (2022), 114958, https://doi.org/10.1016/j.enconman.2021.114958.

[28] A. Klinkova, P. De Luna, E.H. Sargent, E. Kumacheva, P.V. Cherepanov, Enhanced electrocatalytic performance of palladium nanoparticles with high energy surfaces in formic acid oxidation, J. Mater. Chem. A. 5 (2017) 11582–11585, https://doi. org/10.1039/C7TA00902J.

[29] A. Klinkova, P. De Luna, C.-T. Dinh, O. Voznyy, E.M. Larin, E. Kumacheva, E. H. Sargent, Rational design of efficient palladium catalysts for electroreduction of carbon dioxide to formate, ACS Catal. 6 (2016) 8115–8120, https://doi.org/ 10.1021/acscatal.6b01719.

[30] M. Liu, Y. Pang, B. Zhang, P. De Luna, O. Voznyy, J. Xu, X. Zheng, C.T. Dinh, F. Fan, C. Cao, F.P.G. de Arquer, T.S. Safaei, A. Mepham, A. Klinkova, E. Kumacheva, T. Filleter, D. Sinton, S.O. Kelley, E.H. Sargent, Enhanced electrocatalytic CO2 reduction via field-induced reagent concentration, Nature 537 (2016) 382–386, https://doi.org/10.1038/nature19060.

[31] J. Shan, Z. Lei, W. Wu, Y. Tan, N. Cheng, X. Sun, Highly active and durable ultrasmall Pd nanocatalyst encapsulated in ultrathin silica layers by selective deposition for formic acid oxidation, ACS Appl. Mater. Interfaces. 11 (2019) 43130–43137, https://doi.org/10.1021/acsami.9b13451.

[32] M. Mazurkiewicz-Pawlicka, A. Malolepszy, A. Mikolajczuk-Zychora, B. Mierzwa, A. Borodzinski, L. Stobinski, A simple method for enhancing the catalytic activity of Pd deposited on carbon nanotubes used in direct formic acid fuel cells, Appl. Surf. Sci. 476 (2019) 806–814, https://doi.org/10.1016/j.apsusc.2019.01.114.

[33] W. Zhang, Q. Yao, X. Wu, Y. Fu, K. Deng, X. Wang, Intimately coupled hybrid of graphitic carbon nitride nanoflakelets with reduced graphene oxide for supporting Pd nanoparticles: A stable nanocatalyst with high catalytic activity towards formic acid and methanol electrooxidation, Electrochim. Acta. 200 (2016) 131–141, https://doi.org/10.1016/j.electacta.2016.03.169.

[34] J. Nandenha, R.F.B. De Souza, M.H.M.T. Assumpção, E.V. Spinacé, A.O. Neto, Preparation of PdAu/C-Sb2O5·SnO2 electrocatalysts by borohydride reduction process for direct formic acid fuel cell, Ionics (Kiel). 19 (2013) 1207–1213, https:// doi.org/10.1007/s11581-013-0955-5.

[35] S. Yang, Y. Chung, K.-S. Lee, Y. Kwon, Enhancements in catalytic activity and duration of PdFe bimetallic catalysts and their use in direct formic acid fuel cells, J. Ind. Eng. Chem. 90 (2020) 351–357, https://doi.org/10.1016/j. jiec.2020.07.034.

[36] S. Yang, J. Yang, Y. Chung, Y. Kwon, Pd Bi bimetallic catalysts including polyvinylpyrrolidone surfactant inducing excellent formic acid oxidation reaction and direct formic acid fuel cell performance, Int. J. Hydrogen Energy. 42 (2017) 17211–17220, https://doi.org/10.1016/j.ijhydene.2017.06.018.

[37] S.Z. Rejal, M.S. Masdar, S.K. Kamarudin, A parametric study of the direct formic acid fuel cell (DFAFC) performance and fuel crossover, Int. J. Hydrogen Energy. 39 (2014) 10267–10274, https://doi.org/10.1016/j.ijhydene.2014.04.149.

[38] M. Xu, Y. Zhao, H. Chen, W. Ni, M. Liu, S. Huo, L. Wu, X. Zang, Z. Yang, Y.M. Yan, Role of ultrathin carbon shell in enhancing the performance of PtZn intermetallic nanoparticles as an anode electrocatalyst for direct formic acid fuel cells, ChemElectroChem. 6 (2019) 2316–2323, https://doi.org/10.1002/ celc.201900332.

[39] J. Chang, S. Li, L. Feng, X. Qin, G. Shao, Effect of carbon material on Pd catalyst for formic acid electrooxidation reaction, J. Power Sources. 266 (2014) 481–487, https://doi.org/10.1016/j.jpowsour.2014.05.043.

[40] V. Muthukumar, R. Chetty, Morphological transformation of electrodeposited Pt and its electrocatalytic activity towards direct formic acid fuel cells, J. Appl. Electrochem. 47 (2017) 735–745, https://doi.org/10.1007/s10800-017-1076-z.

[41] M. Xu, H. Chen, Y. Zhao, W. Ni, M. Liu, Y. Xue, S. Huo, L. Wu, Z. Yang, Y.M. Yan, Ultrathin-carbon-layer-protected PtCu nanoparticles encapsulated in carbon capsules: A structure engineering of the anode electrocatalyst for direct formic acid fuel cells, Part. Part. Syst. Charact. 36 (2019) 1–10, https://doi.org/10.1002/ ppsc.201900100.

[42] J. Matos, A. Borodzinski, A.M. Zychora, P. Kedzierzawski, B. Mierzwa, K. Juchniewicz, M. Mazurkiewicz, J.C. Hernández-Garrido, Direct formic acid fuel cells on Pd catalysts supported on hybrid TiO2-C materials, Appl. Catal. B Environ. 163 (2015) 167–178, https://doi.org/10.1016/j.apcatb.2014.07.063.

[43] J.K. Yoo, M. Choi, S. Yang, B. Shong, H.-S. Chung, Y. Sohn, C.K. Rhee, Formic acid electrooxidation activity of Pt and Pt/Au catalysts: Effects of surface physical properties and irreversible adsorption of Bi, Electrochim. Acta 273 (2018) 307–317, https://doi.org/10.1016/j.electacta.2018.04.071.

[44] N.V. Rees, R.G. Compton, Sustainable energy: a review of formic acid electrochemical fuel cells, J. Solid State Electrochem. 15 (2011) 2095–2100, https://doi.org/10.1007/s10008-011-1398-4.

[45] T. Wang, A. Chutia, D.J.L. Brett, P.R. Shearing, G. He, G. Chai, I.P. Parkin, Palladium alloys used as electrocatalysts for the oxygen reduction reaction, Energy Environ. Sci. 14 (2021) 2639–2669, https://doi.org/10.1039/D0EE03915B.

[46] X. Huang, Z. Zhao, Y. Chen, C.-Y. Chiu, L. Ruan, Y. Liu, M. Li, X. Duan, Y. Huang, High density catalytic hot spots in ultrafine wavy nanowires, Nano Lett. 14 (2014) 3887–3894, https://doi.org/10.1021/nl501137a.

[47] C. Dong, J. Fu, H. Liu, T. Ling, J. Yang, S.Z. Qiao, X.-W. Du, Tuning the selectivity and activity of Au catalysts for carbon dioxide electroreduction via grain boundary engineering: a DFT study, J. Mater. Chem. A 5 (2017) 7184–7190, https://doi.org/ 10.1039/C6TA10733H.

[48] N.a. Tian, Z.-Y. Zhou, S.-G. Sun, Y. Ding, Z.L. Wang, Synthesis of tetrahexahedral platinum nanocrystals with high-index facets and high electro-oxidation activity, Science 316 (5825) (2007) 732–735.

[49] C. Tang, J. Shi, X. Bai, A. Hu, N. Xuan, Y. Yue, T. Ye, B. Liu, P. Li, P. Zhuang, J. Shen, Y. Liu, Z. Sun, CO 2 reduction on copper's twin boundary, ACS Catal. 10 (2020) 2026–2032, https://doi.org/10.1021/acscatal.9b03814.

[50] W. Huang, A.C. Johnston-Peck, T. Wolter, W.-C. Yang, L. Xu, J. Oh, B.A. Reeves, C. Zhou, M.E. Holtz, A.A. Herzing, A.M. Lindenberg, M. Mavrikakis, M. Cargnello, Steam-created grain boundaries for methane C–H activation in palladium catalysts, Science 373 (6562) (2021) 1518–1523.

[51] D.E. Glass, G.A. Olah, G.K.S. Prakash, Effect of the thickness of the anode electrode catalyst layers on the performance in direct methanol fuel cells, J. Power Sources 352 (2017) 165–173, https://doi.org/10.1016/j.jpowsour.2017.03.106.

[52] K. Dutta, S. Das, D. Rana, P.P. Kundu, Enhancements of catalyst distribution and functioning upon utilization of conducting polymers as supporting matrices in DMFCs: A review, Polym. Rev. 55 (2015) 1–56, https://doi.org/10.1080/ 15583724.2014.958771.